

# Astro2010 Technology White Paper Technology Development Toward Imaging and Spectroscopy of Exo-planets via Visible Nulling Coronagraphic Techniques

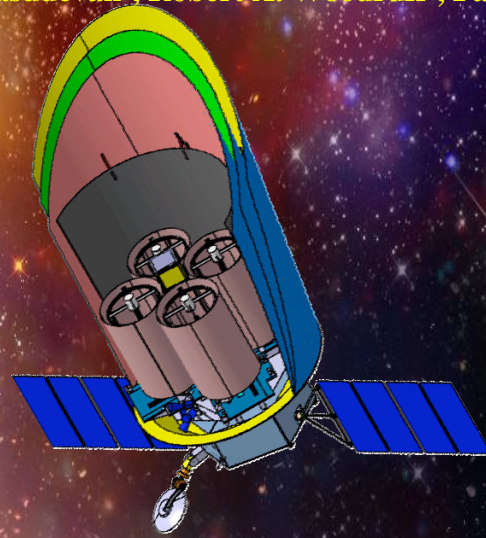
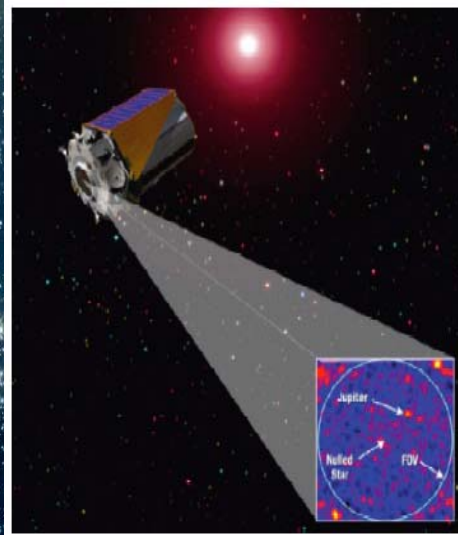
Michael Shao, 818-354-7834 (mshao@jpl.nasa.gov)

Jet Propulsion Laboratory, California Institute of Technology

Mark C. Clampin, 301-286-4532 (Mark.Clampin@nasa.gov)

NASA/Goddard Spaceflight Center, Greenbelt, MD

Peter Lawson<sup>1</sup>, B. Martin Levine<sup>1</sup>, Jagmit Sandhu<sup>1</sup>, Gautam Vasisht<sup>1</sup>, Richard G. Lyon<sup>2</sup>, Benjamin F. Lane<sup>3</sup>, Rocco Samuele<sup>4</sup>, Gopal Vasudevan<sup>5</sup>, Robert A. Woodruff<sup>6</sup>, Fabien Malbet<sup>7</sup>



**Abstract:** The field of Exoplanet research is poised to make major advances in the upcoming decade. One of the more promising approaches for exo-planet detection and spectroscopy over wide wavebands is nulling interferometry, which is capable of producing high contrast images equivalent to  $2\lambda/D$  coronagraphs. When combined with a modest single aperture telescope or a coherent array using 4 telescopes, the nulling interferometer based **visible nulling coronagraph** produces a cost effective instrument for imaging and spectroscopy of over 100 nearby stars. A technology development program is needed to demonstrate the high contrast technique to the required levels of  $10^{-9}$ - $10^{-10}$  contrast. We have already demonstrated nulling levels needed to detect Jovian planets but need further development to demonstrate those of exo-earths. Such development is a continuation of current efforts and is envisioned to be accomplished within 4 year program of testbed demonstration and component development in segmented deformable mirrors and single mode optical fiber array assemblies.

<sup>1</sup> Jet Propulsion Laboratory, California Institute of Technology

<sup>2</sup> NASA/Goddard Spaceflight Center, Greenbelt, MD

<sup>3</sup> C.S. Draper Laboratory, Cambridge, MA 02139

<sup>4</sup> Northrop Grumman Aerospace Systems, Redondo Beach, CA 90278

<sup>5</sup> Lockheed Martin Space Systems Co., Advanced Tech. Center, Palo Alto, CA 94304

<sup>6</sup> Lockheed Martin Space Systems Co., Louisville, CO 80027

<sup>7</sup> University of Grenoble, France

## 1 Introduction and Background

Nearly 350 exo-planets have been discovered. Planets as small as 5 earth masses and two earth diameters (recent Corot discovery) have been found. Astronomers can measure the diameter of planets as they traverse their parent star. Infrared spectra of Hot Jupiters have been measured when those planets have gone behind the parent star in a secondary transit. The next major advance is the discovery and characterization of Earth-like planets in the habitable zone around a parent star.

One of the more promising approaches for exo-planet detection and spectroscopy over wide wavebands is nulling interferometry (Figure 1). A nulling interferometer can be used as a high-contrast imaging system to suppress both diffraction and scattering (Shao, 1991). In principle, a nulling interferometer projects an interference pattern on the sky over the star-planet system being imaged, while the fringe spacing can be tuned for a specific system. The central destructive fringe attenuates starlight and adjacent constructive fringes offer 100% transmission for planet light when the optical path from

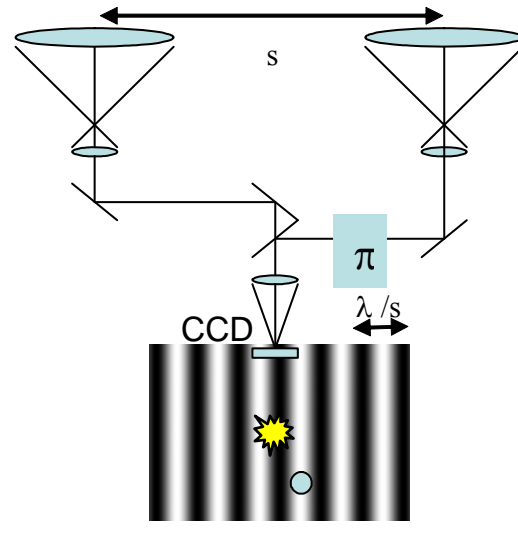


Figure 1: Imaging with a nulling interferometer. A fringe pattern is superimposed over the star and planet to be imaged, the star is placed at the bottom of a deep, achromatic destructive (null) fringe, while planet on the constructive fringe is transmitted.

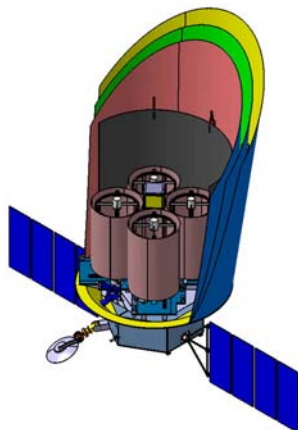


Figure 2: Concept payload for DAVINCI



Figure 3: Concept payload for EPIC

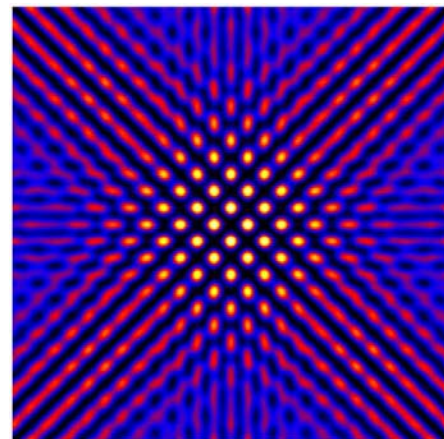


Figure 4: A null pattern at maximum baseline (4m) from 500nm-600nm.

the planet is  $\lambda/2$  different from the star.

In the infrared domain, this approach is known as the Bracewell nulling interferometer (Bracewell and McPhie, 1979). The Dilute Aperture Visible Nulling Coronagraph Imager (DAViNCI) (Shao et. al. 2009), is a large mission concept for exo-planet exploration that uses 4, 1.1m telescopes along a variable baseline (Figure 2). In DAVINCI, we accomplish nulling by coherently combining four separate apertures to produce a null pattern (Figure 4) proportional to the planet angle to the fourth power. The dilute aperture approach breaks the cost paradigm of large monolithic mirrors, and requires 4 telescopes of modest aperture (1.1m ITT, Space Systems LLC NextView-class). DAVINCI has an inner working angle (IWA) equal to an 8m filled aperture telescope that uses a coronagraph ( $IWA \sim 2 \lambda/D$ ).

The Extrasolar Planetary Imaging Coronagraph (EPIC) (Figure 3) is a medium-class mission concept, designed to detect and characterize extrasolar gas giant planets (EGPs), and inventory the architectures of planetary systems (Clampin et. al., 2009). Although it is based on a monolithic 1.65m diameter telescope, both DAViNCI and EPIC's driving technical requirements lie within its instrument, the visible nulling coronagraph (VNC).

In the visible and near infrared, observations can be carried out with conceptually similar variants of the same basic nulling approach using both single aperture telescopes and dilute aperture imaging interferometers. The "nulling coronagraph" creates interference fringes, by shearing a single aperture multiple times (Figure 6), which synthesizes a 4 element long baseline optical interferometer. The baseline is proportional to shear distance, e.g. EPIC). For DAViNCI, the fringes are formed by coherent combination of the four apertures physically separated by their baseline. The nulling approach solves many of the problems associated with normal coronagraphy (like extreme aperture wavefront correction in the mid spatial frequency range, and its ability to interrogate multiple star systems), and also allows smaller, more cost effective telescope apertures to be considered for large scale missions. The VNC architecture is compatible with both obscured and non-obscured telescopes, and is also compatible with segmented telescopes.

EPIC and DAViNCI are designed for direct imaging of gas-giant and terrestrial planets. Using direct imaging in combination with spectroscopy with broad wavelength coverage ( $0.5\mu\text{m}$ - $0.9\mu\text{m}$  for EPIC and  $0.55\mu\text{m}$ - $1.7\mu\text{m}$  for DAViNCI) enables nulling interferometry to address critical scientific questions pertinent to the habitability of terrestrial planets, and to measure biomarkers indicative of life.

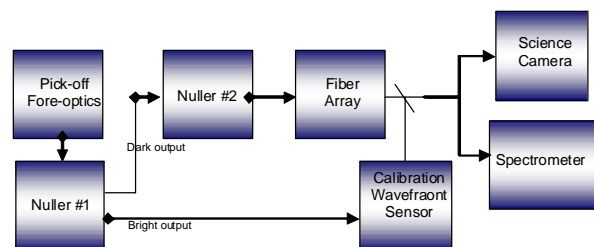


Figure 5: Block diagram of the Visible Nulling Coronagraph.

## 2 Major Components of the Visible Nulling Coronagraph

Light from either the EPIC telescope or the DAViNCI telescopes are sent to the first of two nulling interferometers (Figure 5). There are two outputs, a 'bright' output, whose light is sent to bore sight tracking cameras to minimize jitter during integration and to a calibration wavefront

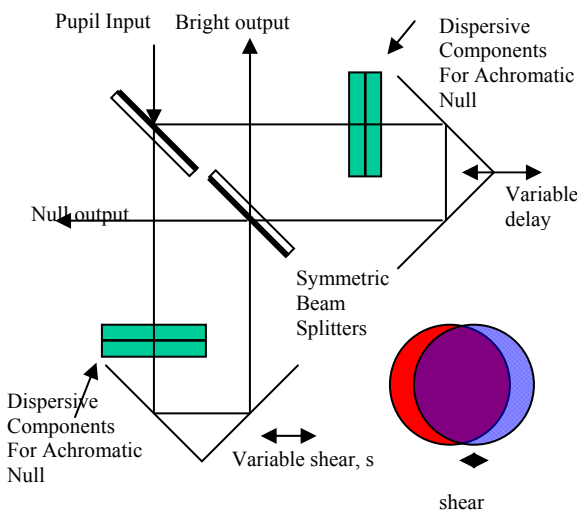


Figure 6: Principal concept for recombination of light from a single telescope. The null output which is then rotated by 90° before input to the second interferometer.

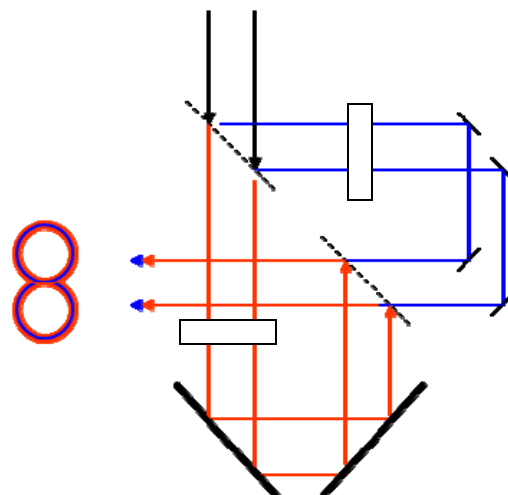


Figure 7: Principal concept for recombination of light from 2 telescopes. There are 2 outputs for each telescope pair which are then combined with the other telescope pair..

sensor, and a ‘dark’ output which is relayed to a second identical nulling interferometer. The dark output of the second interferometer is the fully “nulled” beam, and is spatially filtered by a coherent array of single-mode optical fibers. There are deformable mirrors in each of the nulling interferometers for fine control of amplitude and phase in each fiber of the array. The light from the fiber array is split with one part directed to the planet detection camera (or spectrometer), and the other part sent to the calibration wavefront sensor (DAViNCI only). The calibration wavefront sensor serves as the error signal for the deformable mirrors. EPIC calculates its error signal using a separate null control camera operating from the dark output of the second nuller.

To make the  $\pi$ -radian phase shift achromatic, we use pairs of dielectric plates of differing thicknesses. Solutions for achromatic  $\pi$ -radian phase shifts (to the needed accuracy) exist with two glasses. Thus, for this experiment, the final layout for the beam combiner consists of identical two-glass pairs of rotatable dielectric phase retarders (Morgan et. al., 2003), in each leg of the interferometer (Figure).

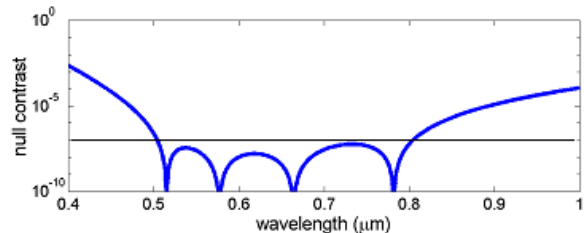


Figure 8: The broad band null depth achievable by using pairs of dielectric plates (Morgan et. al, 2003).

### 2.1 Deformable Mirrors and Single Mode Fiber Arrays

To achieve a deep null, both the amplitude and phase of the interfering wavefronts must be matched to high tolerance in the pupil plane. A deformable mirror (DM) is placed in one arm of each of the nulling interferometers. At the output of the nuller, we use an array of single mode fibers (Figure 9). Within each fiber the electric field is fully specified by two numbers, the phase and amplitude. Each nuller uses a segmented DM, with piston as well as tip/tilt control of each segment. Piston motion controls the phase of the light, while tip/tilt changes the coupling of the light into the single mode fiber. This combination allows us to control both amplitude and phase of the interfering beams in the fiber. At the output of the single mode fiber array, the light from each fiber is collimated. The array of collimated beams is then focused onto a detector (or spectrometer slit). The fiber array is called coherent because the optical paths through all the fibers are matched to 1/4 of a wave.

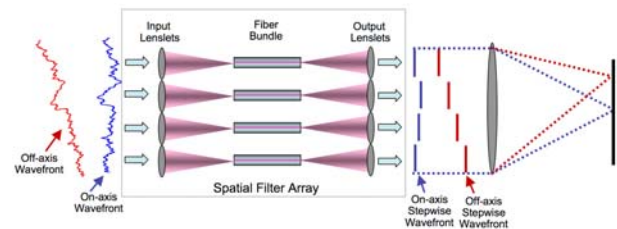


Figure 9. Principal of a Spatial Filter Array. Input wavefront and amplitude aberrations are converted into intensity variations and stepwise phase on output.

### 2.2 Post-coronagraphic Wavefront Sensor (DAViNCI only)

The last element of the instrument is the post coronagraph calibration interferometer (Figure 10). At the output of the fiber array, the starlight should be mostly removed while preserving the planet light. But because we have a dilute aperture, we need to rotate the array, record the data and generate a synthetic aperture image. As the array rotates, the null or stellar leakage from the null has to be stable or precisely measured. The post coronagraph calibration interferometer has two functions, one is to serve as a wavefront sensor to provide feed back to run the DM’s.

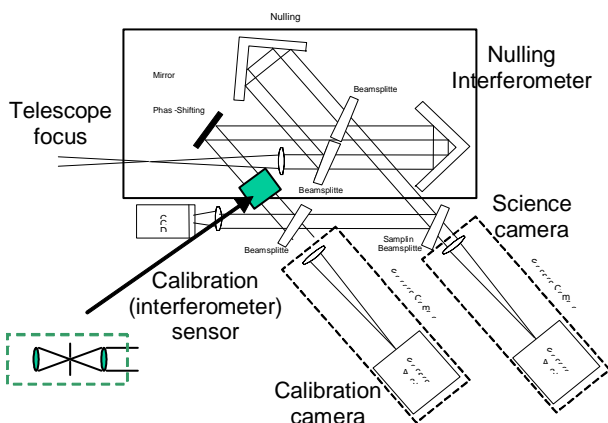


Figure10: Concept for a calibration wavefront sensor with a nulling coronagraph.

The other is to measure the residual starlight leakage. Part of the output of the fiber bundle is interfered with spatially filtered starlight from one of the “bright” outputs of the nulling interferometer. Starlight coming through the “dark” output of the nuller will be coherent with the starlight coming through one of the “bright” outputs, but will not interfere with the local or exo-zodi background. This calibration interferometer concept (Shao, 2007) is also being used in the Gemini Planet Imager, a ground based extreme AO coronagraph, and in PICTURE, a nulling coronagraph on a sounding rocket (50cm telescope). The calibration interferometer was also part of a NASA funded instrument concept study for TPF-C.

### 3 Critical Technology Development

The driving requirements to demonstrate technology readiness come from optical contrast levels of  $10^{-9}$  for Jovian planets and  $10^{-10}$  for earth-sized planets in starlight over an extended field of view. Ultimately we need to show an imaging contrast of  $2 \times 10^{-11}$  over an inner working angle less than 38mas using a wide band pass of starlight (25%). In order to meet this demanding TRL-6 requirement, deformable mirrors, spatial filter arrays and null control algorithms must act together in a stable environment within a vacuum tank.

To image a planet around a nearby star, we need to suppress the light from the star at the position of the planet, down to a level where photon noise from the stellar leakage is smaller than the photon noise from the local and exo-zodi dust. Light at the 1st airy ring is ~2% of its peak intensity. *For DAVINCI, this 2% must be reduced to  $\sim 10^{-9}$  to be below the local/exo-zodi.* Residual stellar speckles are still ~10X brighter than the planet. Next we need a method for measuring the residual starlight speckle pattern (wavefront calibration), down to ~1/5 of the planet light, meaning the residual speckles must be subtracted to  $\sim 2 \times 10^{-11}$  for a Earth @  $10^{-10}$  contrast.

We have divided the technology tasks into **wide band starlight suppression** and **demonstration of high contrast imaging** using the VNC over an extended field of view. These demonstrations run concurrently with component development of **segmented deformable mirrors** and **fabrication of coherent single mode fiber arrays**.

#### 3.1 Wide bandwidth starlight suppression:

We have already achieved a deep,  $10^{-6}$  null over a wide 16% spectral band (Samuele et. al, 2007) (Figure 11). When combined with a 1000 element single mode fiber array, this would yield a  $10^{-9}$  contrast. The major challenge of achieving deep starlight suppression is the precise control of both amplitude and phase. The residual  $10^{-6}$  leakage is due in part to phase errors and in part to amplitude errors, while the optical path in the two arms is matched to ~40 picometers, and the intensity difference of the two interfering beams is matched to 0.06%. These

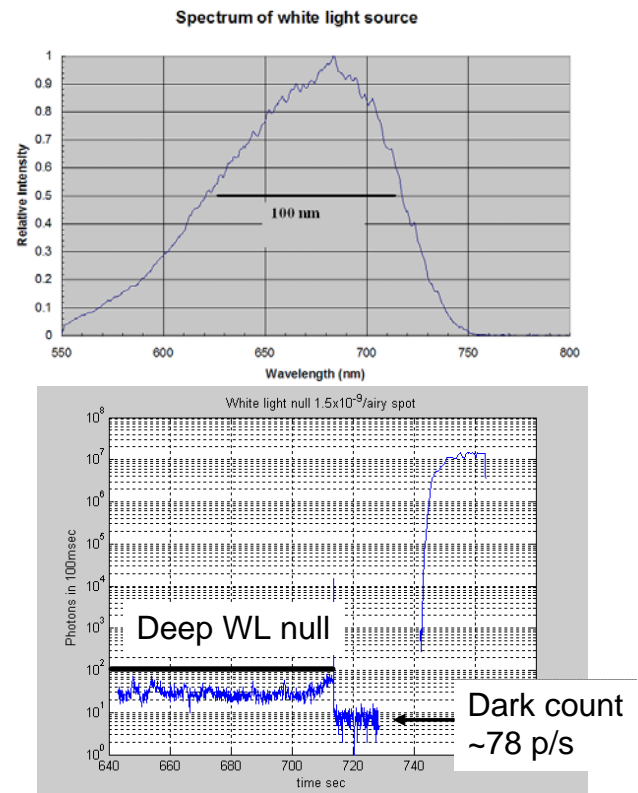


Figure 11: (Upper) The 15% white light spectrum after propagation through one arm of the interferometer. The Full width at half maximum is 100 nm. (Lower) The resulting null plot showing  $10^{-6}$  starlight suppression.

measurements were made with the interferometer in the quiescent environment of a vacuum chamber, but at atmospheric pressure. This level of performance is satisfactory for EPIC but needs another factor of 2-3 for DAViNCI.

Starlight suppression of  $10^{-6}$  is required to produce an overall contrast of  $10^{-9}$  (suitable for DAViNCI). (Earth-like planets) at an equivalent angle of  $1-2\lambda/D$ . Final image contrast needs to be achieved with using the calibration wavefront sensor data to subtract speckles to the  $2 \times 10^{-11}$  contrast level (5x lower than an Earth planet contrast of  $10^{-10}$ )

### 3.2 High Contrast Imaging

To achieve this we need a test bed that is capable of demonstrating starlight suppression over a multiple 'pixel' field of view. In the DAViNCI and EPIC architectures, the output of the nuller is coupled to a coherent array of optical fibers in the pupil plane. Each segment of the segmented DM controls the amplitude and phase into one fiber in the array. The output of the fiber array is focused onto the science camera as in Figure 12. Both JPL and GSFC are developing parallel test beds. Significant advances have occurred at GSFC in the development of an imaging test bed with null control

algorithms resulting in stable closed-loop control in a noisy lab environment at 6.7 Hz.

The APEP Optical test bed is designed for a vacuum environment (Figure 12). It will be capable of remote access, so both JPL and GSFC will be able to use the test bed to demonstrate high contrast imaging and also demonstrate control algorithms.

The nulling interferometer with a DM, and calibration wavefront sensor are shown. The fiber array is not yet shown. It will be located in front of the 400mm achromatic lens before the science camera.

APEP is an advanced testbed that will ultimately demonstrate high contrast imaging to the required levels for both EPIC and DAViNCI.

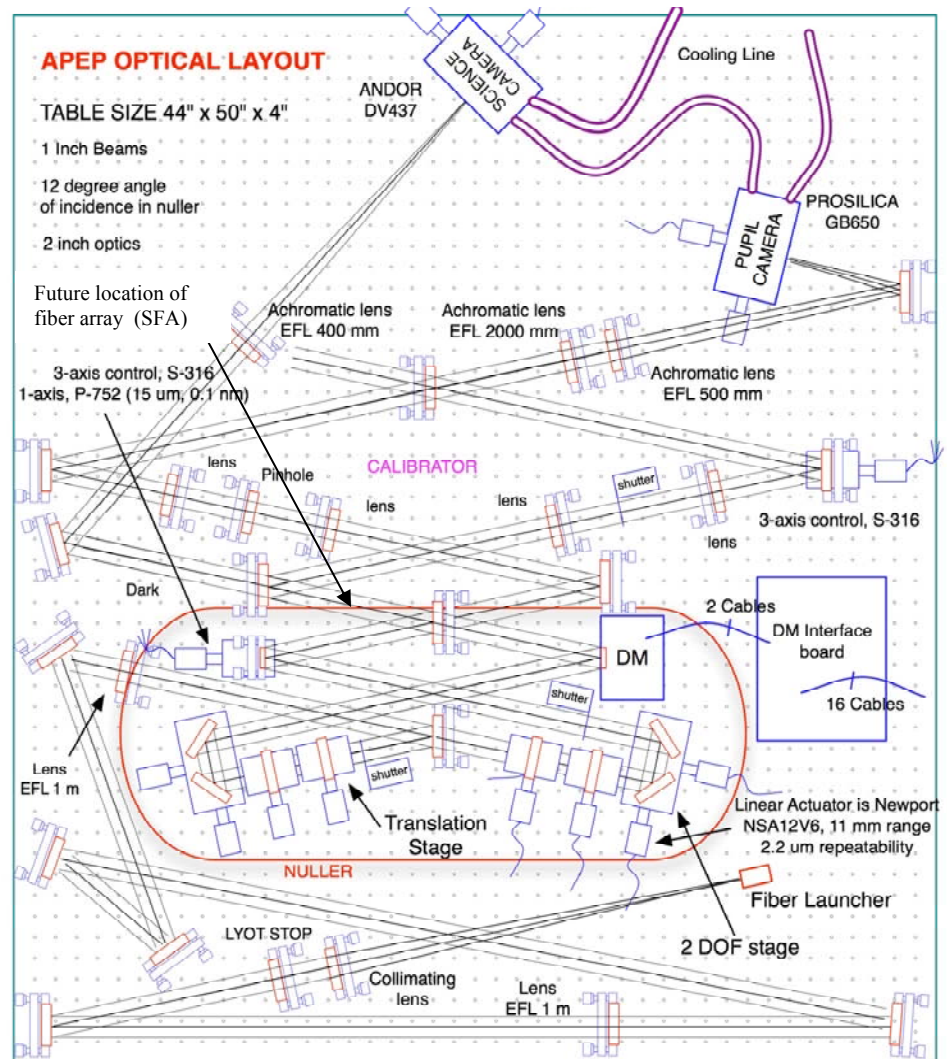


Figure 12: JPL Nulling Test bed for demonstration of high contrast imaging using a nulling interferometer, DM, fiber array, and with a post-coronagraphic wavefront sensor.

### 3.3 Component Development

#### 3.3.1 Deformable Mirror Technology

The deformable mirror consists of hexagonal mirror segments, each having 3 degrees of freedom. The Boston Micromachines Corp (BMC) concept (Figure 13) uses three actuators connected to the hexagonal mirror segment via posts that resemble vertices of an equilateral triangle. This actuator geometry provides the mirror with unlimited degrees of tip/tilt motion, and when the actuators are deflected by equal amounts, the mirror segment can be moved in piston. The mirror segments are designed to have  $1\mu\text{m}$  of piston stroke when they are tilted to  $3\text{mrad}$ . In other words, if the mirror elements remained flat, the mirror could experience  $2\mu\text{m}$  of piston motion before reaching the actuator limit. However,  $1\mu\text{m}$  of this motion is reserved for tip/tilt behavior.

IRIS AO is developing a deformable mirror that is a hybrid of surface micromachining and bulk micromachining (Figure 14).

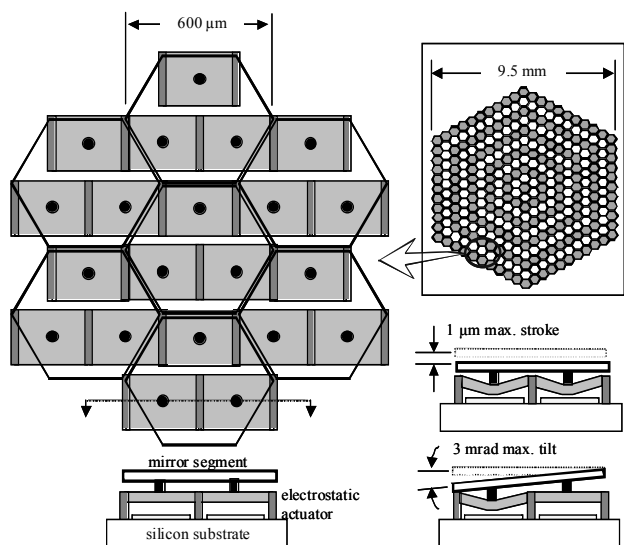


Figure 13: Top and side view of the BMC MEMS DM architecture for tip/tilt and piston motion (left).

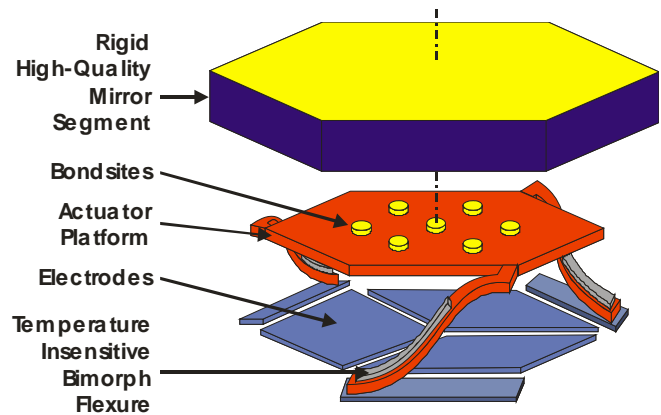


Figure 14: Diagram of a single Iris AO mirror segment. Dozens or even thousands of these of these may be tiled into a deformable array

Under TPF funding, Boston Micromachines Corporation (BMC) developed an architecture for a segmented deformable mirror and produced a 61 segment demonstrator. The main drawback was that

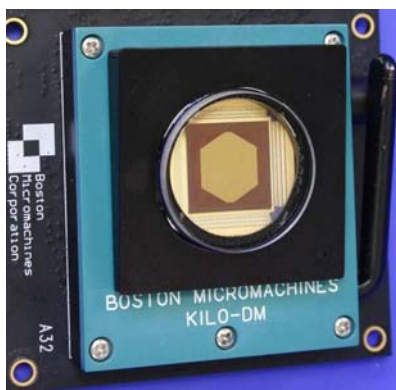


Figure 15: 331 Segmented DM technology demonstrator

the segments were not uniformly flat. Under subsequent SBIR funding, BMC has mitigated this problem and has delivered a 331 segment deformable device (Figure 15 and Stewart et.al, 2007). They have demonstrated segment flatness to  $4\text{m}$  radius of

curvature and  $5\text{nm}$  rms roughness. Figure 16 shows the mirror response to each of its three actuators per segment.

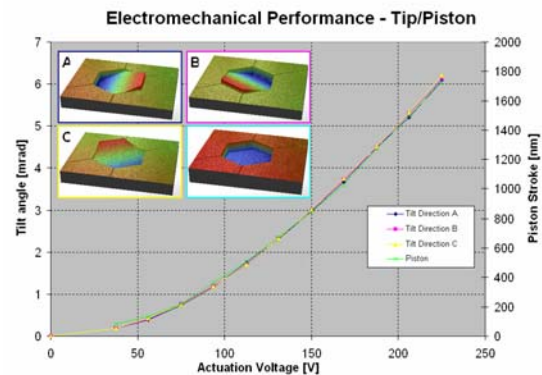


Figure 16: Performance characterization of 331 segment deformable mirror for each actuator separately and for all actuators together.

Also under SBIR funding Iris AO is developing a DM through a combination of fabrication techniques resulting in a DM that has demonstrated 7.6 $\mu$ m of stroke at 125V, 98.6% fill factor, and optical quality of better than 16nm of rms after packaging. Preliminary cyclic tests over 110 hours and 10<sup>7</sup> cycles show no noticeable changes to the actuator positions after cycling (Figure 17).

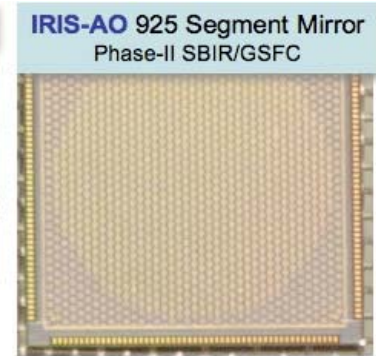
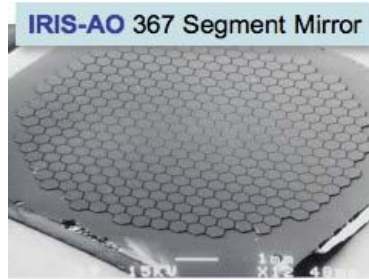


Figure 17: Current state of development of Iris AO segmented deformable mirrors.

Hexagonal mirror segments are tiled to form a DM array. Thick (20 $\mu$ m)

single crystal silicon mirror segments are assembled onto surface micromachined platforms using flip chip bonding. The rigid segments maintain high optical quality (<20nm rms figure

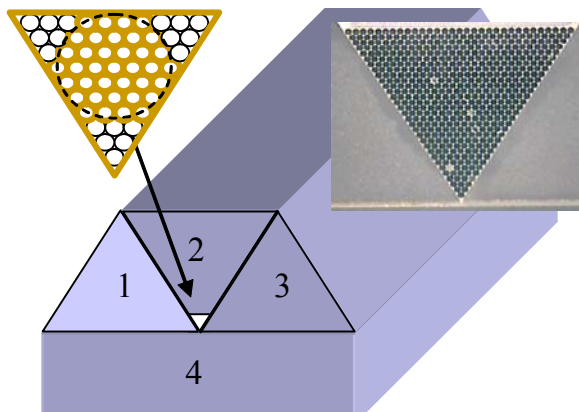


Figure 18: Fiber array is made by confining fibers by equilateral prisms 1 and 3 and equilateral prism 2 with one vertex beveled (polished off) to have a width given by that of the fiber array plus the diameter of one fiber.

errors) after packaging. Each actuator platform is anchored to the chip substrate via three bimorph flexures that elevate them after release because of engineered residual stressing in the top material of the bimorph flexure. The top layer of high stress material bends the polysilicon suspension into position. The three underlying electrodes allow for piston motion when energized with equal voltages and tilt motions when energized with different voltages (Helmbrecht et. al., 2006). They have delivered a 367 segment demonstration mirror and a 925 segment demonstration mirror proving that this architect is capable of fabrication at flight like sizes (Figure 17). Current funding is devote toward fabrication of a 163 segment fully functional mirror. Future work will concentrate on producing an interconnect scheme to provide electrical access to all

actuators, and to develop a lower segment surface error.

Although key technology requirements have been met by both BMC and Iris AO, future development will work toward realizing 1000 segment deformable mirrors with no dead actuators with both architectures.

### 3.3.2 Fiber Optic Array Technology

The JPL fiber array design uses three precision equilateral prisms placed on a flat base plate as shown in Figure 18 (Liu et. al, 2005). The middle prism has one of its vertices polished flat to a width approximately equal to the side length of the fiber array. The fiber array is confined by two facing sides of the upright prisms and the flat top of the middle prism.

The state of the art in Fiber optic arrays is also a 331 hexagonal array of single mode fibers. The key technology challenge has been to align and bond a lens array to this fiber array to produce a single monolithic assembly.

Both GSFC and JPL are working with Fiberguide Industries to develop such a custom subscale monolithic assembly consisting of 217-fibers which is specified to meet all the

requirements for flight except for the number of fibers (Figure 19). It is expected that two units will be delivered (one to GSFC and one to JPL) by the end of 2009.

In addition GSFC has an ongoing phase-I SBIR to develop an alternative waveguide based approach. We need to develop an integrated array with 1000 fibers for the ultimate flight instrument, and successful demonstration of these subscale technologies is the first important step.

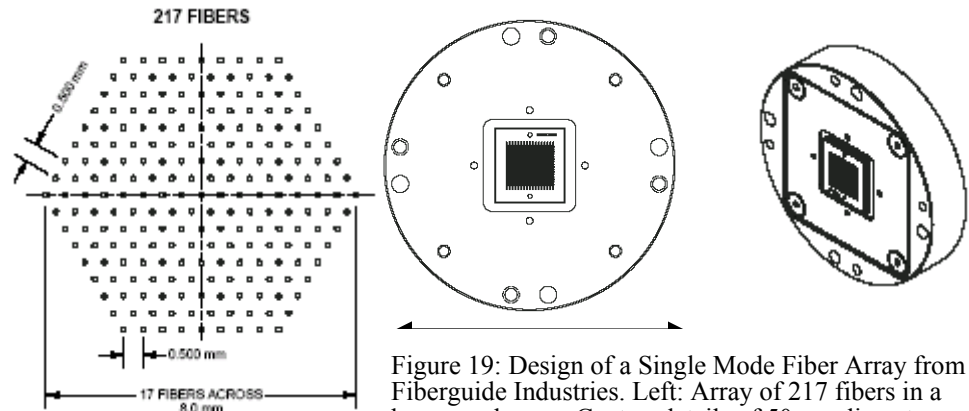


Figure 19: Design of a Single Mode Fiber Array from Fiberguide Industries. Left: Array of 217 fibers in a hexagonal array. Center: details of 50mm diameter end face. Right: View of 1cm thick array.

## 4 Cost and Schedule

The technology development schedule is given below in Figure 20. It includes time for test bed integration and demonstration of high contrast imaging milestone of  $10^{-8}$ ,  $10^{-9}$ , and  $10^{-10}$  contrast. Concurrent with the test bed is the development of 1000 segment deformable mirrors and matching single mode fiber arrays. The test bed development program is currently under NASA funding. This includes funding for initial SFA development. The deformable mirrors have previously all been developed under SBIR funding.

Our costing estimate is notional and based on current levels of effort. Assuming a 4 year program starting in FY2011, the test bed would request support of 5 FTE + the cost of equipment. Historically each deformable mirror has been developed for \$750K under the SBIR program, and each fiber array costs \$100K. We recommend 2 vendors each of DM and SFA technologies. So the total cost of the technology program would be 4 years x 5-10 FTE + equipment + deformable mirror development costs + fiber array development costs. The total cost is roughly \$10-\$20M.

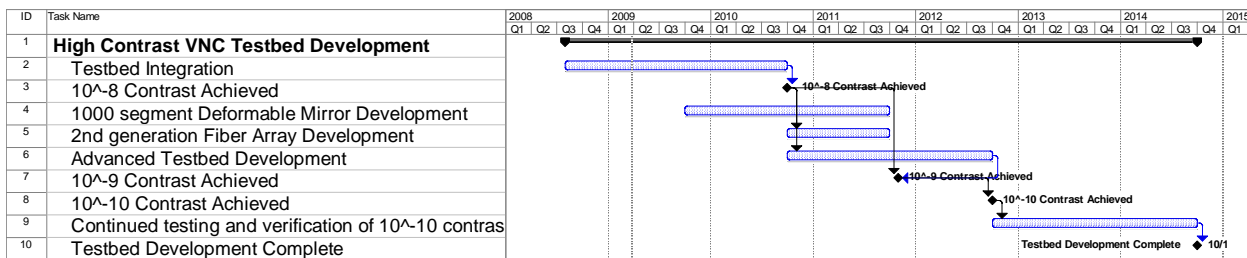


Figure 20: Visible Nulling Coronagraph Technology Development and Mission Implementation Schedule

## 5 Recommendations

We recommend a technology development program to demonstrate the levels of contrast needed for the imaging earth-like exo-planets and spectroscopic investigations of their atmospheres. Starlight suppression of  $10^{-6}$  is required to produce an optical contrast of  $10^{-9}$  Final image contrast after speckle subtraction needs to be  $2 \times 10^{-10}$  for Jovian planets, and  $2 \times 10^{-11}$  for

Earth-like planets at an equivalent angle of  $1-2\lambda/D$ . This is ultimately achieved with using the calibration wavefront sensor data to subtract speckles to their required levels.

*Optical nulls using a single mode fiber have already been demonstrated to  $10^{-7}$  in laser light and  $10^{-6}$  in broad band light. These levels are acceptable within a factor of 2 for EPIC and within an order of magnitude for DAVINCI.* Optical contrast has yet to be demonstrated with the combination of the nulling architecture (including the calibration wavefront sensing system).

Future demonstrations would support medium class missions such as EPIC and the final demonstration would support large missions such as DAVINCI. We need advanced test beds in vacuum to demonstrate the required contrast levels. Concurrent with these demonstrations are technology development in segmented deformable mirrors and single mode fiber arrays. Vendors have shown that 1000 segment DM's can be fabricated. To date, we have 300 segment subscale devices available for test. We have also shown that large fiber arrays can be built, but they also need to be integrated with lens arrays to form a monolithic module. We recommend a 4 year technology development program, to fabricate full scale DM's and fiber arrays, and to perform demonstrations of the ultimate contrast levels. Such a program would cost less than \$20M.

## 6 References

---

- Bracewell R.N., and McPhie R.H., *Icarus*, Vol. 38, 136,1979
- Helmbrecht, M.A., Juneau, T., Hart, M., and Doble, N., (2006) Performance of a high-stroke, segmented MEMS deformable-mirror technology, *Proc. SPIE*. v6113
- Clampin, M., (2009), *Extrasolar Planetary Imaging Coronagraph (EPIC)*, Paper 234.06, 213<sup>th</sup> AAS, Long Beach, CA.
- Liu, D.T., et.al., (2005), "Single Mode Fiber Array for Planet Detection using a Visible Nulling Interferometer", *Proc. IEEE Big Sky Conference*.
- R. G. Lyon, et. Al., *Nulling Coronagraphy for Exo-Planetary Detection and Characterization*, IAU, October 2005, Nice France
- Morgan, et. al., (2003), *Final laboratory results of visible nulling with dielectric plates*, *SPIE v 4838*.
- Samuele, R., et. al., (2007). "Experimental Progress and Results of a Visible Nulling Coronagraph" *IEEE Paper #1366*.
- Shao, M., (2007), "Calibration of residual speckle in a nulling coronagraph", *Comptes Rendus Physique*, Volume 8, Issues 3-4, April-May 2007, Pages 340-348.
- Shao, M., Principal Investigator, (2006), 'TPF-C Instrument Concept Study, Visible and Infrared Nulling Coronagraph Spectrometer', A Report Submitted to the Terrestrial Planet Finder Coronagraph Science and Technology Development Team 7 March 2006, p4.,.
- Shao, M., (2009a), *DAVINCI a Dilute Aperture Coronagraph*, Paper 234.05, 213<sup>th</sup> AAS, Long Beach, CA.
- Shao, et.al., (2009b), 'Direct Detection and Spectroscopy of Exo-Earths; The Need for High Angular Resolution and Other Observational Requirements', <http://www8.nationalacademies.org/astro2010/publicview.aspx>.
- Stewart, et.al., (2007), *Design and development of a 331-segment tip-tilt-piston mirror array for space-based adaptive optics*, *Sensors and Actuators A 138*, pp. 230-238.

**Acknowledgments:** This research was carried out at the Jet Propulsion Laboratory, California Institute of Technology, under a contract with the National Aeronautics and Space Administration. ©2009. All rights reserved.